To appear in the *International Journal of Remote Sensing*
Vol. 00, No. 00, Month 20XX, 1–19

GUIDE

An effective hybrid approach to remote sensing image classification

(*Received 00 Month 20XX; accepted 00 Month 20XX*)

The paper presents a hybrid fuzzy classifier for effective land use land cover mapping. It discusses a Bayesian way of incorporating spatial contextual information into the Fuzzy Noise Classifier (FNC). The FNC was chosen, as it detects noise using spectral information more efficiently than its fuzzy counterparts. The spatial information at the level of second order pixel neighbourhood was modelled using Markov Random Fields (MRFs). Spatial contextual information was added to the MRF using different adaptive interaction functions. These help to avoid over-smoothening at the class boundaries. The hybrid classifier was applied to Advanced Wide Field Sensor (AWiFS) and Linear Imaging Self Scanning Sensor-III (LISS-III) images from a rural area in India. Validation was done with a Linear Imaging Self Scanning Sensor-IV (LISS-IV) image from the same area. The highest increase in accuracy among the adaptive functions was equal to 4.1% and 2.1% for AWiFS and LISS-III images, respectively. The paper concludes that incorporation of spatial contextual information into the fuzzy noise classifier helps in achieving a more realistic and accurate classification of satellite images.

Keywords: Noise; Classification; Markov Random Field; Simulated Annealing, Fuzzy Error Matrix

1. Introduction

Image classification is widely applied in image analysis to extract land use and land cover information from remote sensing images. Conventional classification used the spectral information from a single pixel, i.e. its DN value. It was based upon the rather unrealistic assumption that pixels are pure, i.e. a pixel is the reflected value of a single class (Zhang and Foody, 1998). In the nineteen eighties, fuzzy classifiers were developed for addressing heterogeneity within a pixel, as a mixed pixel, thus improving the accuracy and making classification more realistic (Bezdek et al., 1984). Fuzzy classifiers generate fractional images, i.e. one image for every class, representing the associated membership values at the pixel level. Fuzzy c-Means (FCM) classification is a popular fuzzy classification technique based on fuzzy set theory (Zadeh, 1965). It is, however, sensitive to noise and outliers due to the probabilistic constraint involved (Krishnapuram and Keller, 1993). Possibilistic c-means (PCM) classification addresses this sensitivity problem by redefining the concept of membership values. Membership values generated by a PCM classification represent the degree of belongingness of a pixel to a class, rather than the degree of sharing of classes within a pixel, as was the case with FCM. For this reason, PCM performs better in the presence of noise and outliers (Krishnapuram and Keller, 1996).

Noise in remote sensing images arises due to sensor deficiencies, data processing errors, atmospheric noise and presence of classes other than the class of interest.

The presence of such noise in a remote sensing image degrades the classification accuracy. Noise clustering (NC) is robust against noisy data and has been used successfully in various fields (Dave, 1991). It groups all noisy pixels in a separate class called the noise class based on their spectral properties. Image noise is often found as unrealistic pixel values at unexpected locations and is commonly referred to as the Isolated Pixel Problem (IPP). Spectral classifiers do not entirely address the IPP as they refer only the digital number of image pixels for achieving image classification (Krishnapuram and Keller, 1993). The suitable use of context allows the elimination of possible ambiguities, the recovery of missing information, and the correction of errors, thus improving the robustness of a spectral classifier against noise (Li, 1995; Magnussen et al., 2004). By providing NC with additional information, e.g. information about the neighbourhood classes for a pixel, the classifier would be more accurately predicting the class to which a noisy point belong.

In remote sensing, the energy reaching the sensor does not entirely correspond with the pixel area on the ground, as it also includes energy from neighbouring pixels areas. This is mostly caused by diffuse scattering of the incoming radiation due to atmospheric distortion. Moreover, classes on the ground usually span several pixels and it is rare to find a class in isolation. Hence, there exists a relation between a pixel and its neighbouring pixels. Markov random fields (MRFs) are used in effective modelling of such contextual relationships, in the case of context-dependent entities such as image pixels (Geman and Geman, 1984; Li, 2009). It has been widely used in image segmentation and image restoration (Derin and Elliott, 1987; Dubes and Jain, 1989; Tso and Olsen, 2005). MRFs based upon simulated annealing optimization (Mather, P. and Tso, B., 2010) have been widely accepted for modelling contextual information in images, since the classical paper by Geman and Geman (1984). It considerably improved the accuracy of PCM (Chawla, 2010) and FCM (Singha et al., 2015) classifiers. In those studies, modelling of spatial contextual information was done using both the smoothness prior MRF model (S-MRF) and four different discontinuity adaptive MRF models (DA-MRF)(Li, 2009). Among these models, the use of DA-MRF models helped to produce a higher classification accuracy as compared with S-MRF models (Chawla, 2010; Singha et al., 2013).

Accuracy assessment of a fuzzy classification is not straightforward, because multiple classes might be assigned to a single pixel and so the standard error matrix cannot be realized (Silván-Cárdenas and Wang, 2008). Efforts to assess the accuracy of a fuzzy classification result after making it crisp, resulted in loss of information (Foody, 1997; Silván-Cárdenas and Wang, 2008). Various suggestions have been provided to carry out a fuzzy image accuracy assessment (Binaghi et al., 1999; Congalton, 1991; Green and Congalton, 2004; Pontius Jr. and Cheuk, 2006), but a standard accuracy assessment technique is still missing. Among the various methods proposed, the fuzzy error matrix (FERM) has been widely accepted and hence was used in this study for accuracy assessment (Binaghi et al., 1999).

The aim of this paper is to present a novel hybrid fuzzy noise classifier, and then study its effects on the classification accuracy. Here, the spatial contextual information was modelled using MRFs and thus incorporated into the fuzzy noise classifier, hence creating a novel hybrid classifier. This classifier was applied on Advanced Wide Field Sensor (AWiFS) and Linear Imaging Self Scanning Sensor-III (LISS-III) images from the Resourcesat-1 satellite on the Uttarakhand state in India. Results were evaluated with a Linear Imaging Self Scanning Sensor-IV (LISS-IV) image.

The outline of the paper is as follows. An algorithmic overview of the noise clustering is explained in section 2. Section 3 describes the methodology used in this paper and section 4 describes the study area and image used for the study. The results from the study is included in section 5, followed by a discussion of the results in section 6.

2. Noise clustering

The presence of noise is often perceived as a problem for effective clustering, as it biases clustering algorithms and results in formation of unrealistic clusters. Noise clustering is a fuzzy clustering technique which was developed to address this problem. It overcomes the possible problem of unrealistic cluster formation due to presence of noise in the input image (Dave, 1993; Krishnapuram and Keller, 1993) It achieves this immunity to noise, by allocating noisy data into a separate class called as the noise class. The noise class cluster center is selected such that it is equidistant from all the points in the image, thus each data point in the noise cluster has an equal prior probability of belonging to any other cluster. In noise clustering, data points beyond the noise distance (δ) from the cluster centers are considered as noise, but the pre-specification of (δ) is not practical due to lack of enough information about the data (Dave, 1991). In this study, the (δ) was estimated using the method mentioned in section 3.2. The figure 1(a) shows sample data set taken from (Dave, 1993) and the figure 1(b) shows the result of noise clustering on the image. Three valid clusters formed by noise clustering are represented in Figure 1(b) using unique symbols whereas the '+' symbol represents the noisy data assigned to the noise class.

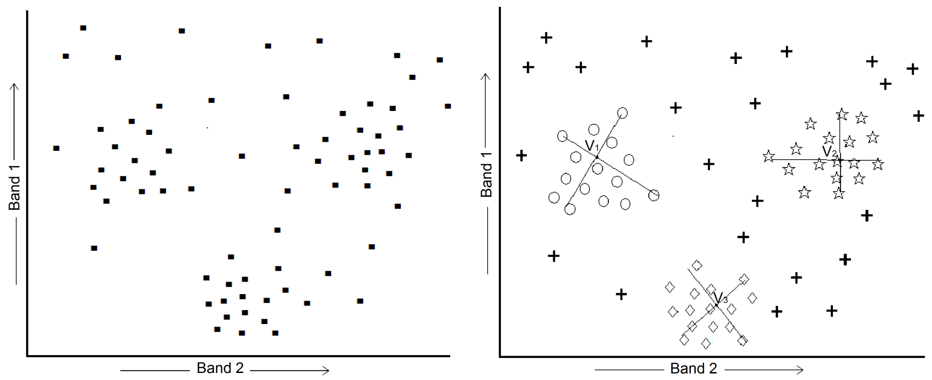

(a) Noisy data (b) Clusters Identified using noise clustering

Figure 1.: An example of cluster formation using noise clustering for $C = 3$ classes and two spectral bands. In b) the '+' indicates the noise class.

Mathematically, noise clustering is modelled as an optimization problem with (1) as its objective function that needs to be minimized, and (2) as its constraint.

$$\mathrm{J}_{\mathrm{NC}}(U;V) = \sum_{i=1}^{N}\sum_{j=1}^{C}(u_{ij})^m \mathrm{d}(\vec{\boldsymbol{x}}_{\boldsymbol{i}}, \vec{\boldsymbol{v}}_{\boldsymbol{j}}) + \sum_{i=1}^{N}(u_{i,c+1})^m\delta \tag{1}$$

$$\sum_{j=1}^{C+1} u_{ij} \leq 1 \quad 1 \leq i \leq N \tag{2}$$

In (1), C is the number of classes, N is the total number of image pixels , m is the fuzzification factor, u_{ij} is the membership value of the i^{th} pixel to the j^{th} class and $u_{i,c+1}$ corresponds to the membership values of the noise class. Further, $\vec{\boldsymbol{v_j}}$ denotes the vector pointing to the cluster center of the j^{th} class and $\vec{\boldsymbol{x_i}}$ is the membership value vector for the i^{th} pixel. The Euclidian distance between $\vec{\boldsymbol{x_i}}$ and $\vec{\boldsymbol{v_j}}$ is represented by $\mathrm{d}(\vec{\boldsymbol{x_i}}, \vec{\boldsymbol{v_j}})$. Both $\vec{\boldsymbol{x_i}}$ and $\vec{\boldsymbol{v_j}}$ are vectors in a D dimensional feature space, where D is the number of bands in the input image. The constraint $\sum\limits_{j=1}^{C+1} u_{ij} \leq 1$ allows the noisy data to achieve as small a membership values as possible (Davé and Krishnapuram, 1997). The cluster centers are jointly represented by the set V $= \{V_1, V_2, \ldots, V_C\}$, where $V_1, V_2, \ldots, V_C$ represent the cluster centers for the $1^{\text{st}}, 2^{\text{nd}}, \ldots, C^{\text{th}}$ class. The set U $= \{U_1, U_2, \ldots, U_C, U_{C+1}\}$ contains the membership values for individual classes, where $U_1, U_2, \ldots, U_C$ represent the set of membership values for each pixel in the image and for each class, and U_{C+1} represents the set of membership values for the noise class. The value of the membership values u_{ij} , membership values for noise class $u_{i,c+1}$ and class mean vectors $\vec{\boldsymbol{v_j}}$, can be obtained from the equations (3), (4) and (5) respectively.

$$u_{ij} = \left[\sum_{k=1}^{C} \left(\frac{\mathrm{d}(\vec{\boldsymbol{x_i}}, \vec{\boldsymbol{v_j}})}{\mathrm{d}(\vec{\boldsymbol{x_i}}, \vec{\boldsymbol{v_k}})} \right)^{\frac{1}{m-1}} + \left(\frac{\mathrm{d}(\vec{\boldsymbol{x_i}}, \vec{\boldsymbol{v_j}})}{\delta} \right)^{\frac{1}{m-1}} \right]^{-1} \tag{3}$$

$$u_{i,c+1} = \left[\sum_{i=1}^{C} \left(\frac{\delta}{\mathrm{d}(\vec{\boldsymbol{x_i}}, \vec{\boldsymbol{v_j}})} \right)^{\frac{2}{m-1}} + 1 \right]^{-1} \tag{4}$$

$$\vec{\boldsymbol{v_j}} = \frac{\sum\limits_{i=1}^{N} \left((u_{ij})^m \, (\vec{\boldsymbol{x_i}}) \right)}{\sum\limits_{i=1}^{N} (u_{ij})^m} \tag{5}$$

In this paper a supervised version of the noise clustering, referred to as the fuzzy noise classifier (FNC), was used. The cluster centers V were initialized with the class mean vectors obtained from the supervised approach. i.e. for each class, random pixels were selected and pixel vectors were averaged to produce a mean vector. This also gives a computational advantage for the FNC as it reduces the number of iterations required to reach the optimal cluster centers, whereas it also ensures reproducibility of the results. More intuition on the need of cluster initialization can be obtained on understanding the NC objective function (1), which aims to minimize U and V simultaneously.

3. Methodology

The objective of this study was to develop an efficient hybrid classifier by integrating spatial contextual information onto the fuzzy noise classifier which uses only the spectral information to perform classification. To achieve this, an integral part of the methodology was to formulate the objective functions for the $\mathrm{FNC_S}$ and four $\mathrm{FNC_{DA}}$ classifiers. Estimation of the parameters of the FNC and the parameters of the hybrid classifier were carried out to ensure optimal performance. The accuracy assessment of the hybrid classifier, which is also a fuzzy classifier was done using the FERM. The figure 2 shows the methodology used in this paper.

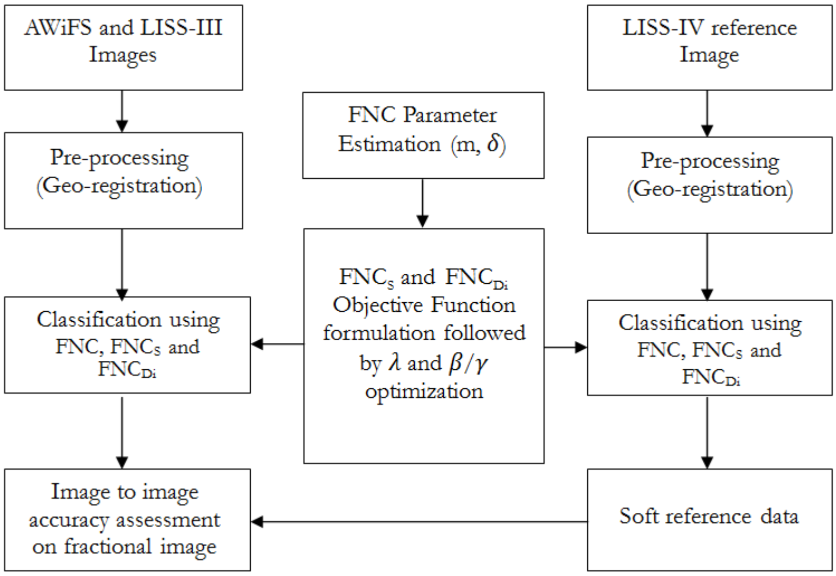

Figure 2.: Methodology followed in this manuscript. On the left side are the AWiFS and LISS-III images used to study the hybrid classifier performance, on the right side is the LISS-IV image used for validation. All terms are defined in the text.

Over-smoothening at the boundaries in an image, on using smoothness (S) MRF priors, was addressed in this study by replacing it with discontinuity adaptive (DA) MRF priors. These use an Adaptive Interaction Function (AIF) $\mathrm{h}(\eta)$, as a function of η, that is placed within the regularizer to model the nature of the interaction of a pixel site with its neighbours. The η represents the difference in membership values between the center pixel and its neighbour within a clique. A clique is a subset of site from the neighbourhood system, where the members of the site are mutual neighbours (Mather and Tso, 2010). The $\mathrm{h}(\eta)$ returns a small value when the membership variation in the pixel neighborhood is large, and returns a large value when the membership variation in the pixel neighborhood is small, resulting in selective smoothening. The equation (6) shows the relation between, the AIF, $\mathrm{h}(\eta)$ and the Adaptive Potential Function (APF), $\mathrm{g}^{'}(\eta)$. The APF encodes the neighbourhood information for a pixel, and it is further incorporated in the objective function of the FNC to form the hybrid classifier.

$$\mathrm{g}^{'}(\eta) = 2\eta\mathrm{h}(\eta) \tag{6}$$

Four AIFs from the literature are used in this work (equation (7) - (10)), resulting in four different APF's and hence four different DA models (Li, 2009). Each AIF has a unique response graph, and in this way models the interaction between a pixel site and its neighbours in a different way. In equations ((7) - (10)), the parameter γ, controls the intensity of the interaction between a pixel and its neighbours. Incorporation of each of these APF's onto the objective function of FNC created a new hybrid classifier, and are referred to in this paper as DA_1, DA_2, DA_3 and DA_4 MRF models, respectively.

$$\mathrm{h}_1(\eta) = \exp \frac{-\eta^2}{\gamma} \tag{7}$$

$$\mathrm{h}_2(\eta) = \frac{1}{\left[\frac{1}{1+\frac{\eta^2}{\gamma}}\right]^2} \tag{8}$$

$$\mathrm{h}_3(\eta) = \frac{1}{1+\frac{\eta^2}{\gamma}} \tag{9}$$

$$\mathrm{h}_4(\eta) = \frac{1}{1+\frac{|\eta|}{\gamma}} \tag{10}$$

3.1. *Mathematical formulation of hybrid classifiers*

The FNC achieves classification by solving an optimization problem, as stated by equations (1) and (2). The hybrid classifiers was created by adding a spatial term to the objective function of the FNC, while keeping its optimization problem constraint unchanged. Spatial contextual information was modelled using all four different DA-MRF models mentioned in section 3, separately. Modelling was also done using the S-MRF model for showing the performance improvement of the classifier against the four DA-MRF models. Using Bayes theorem we were able to incorporate the spatial information modelled using MRFs into equations (1), hence formulating the objective function for the hybrid classifier.

The formulated objective function of $\mathrm{FNC_S}$ classifier is shown in equation (11):

$$\mathrm{E}\left(u_{ij}\right) = (1-\lambda)\left[\sum_{i=1}^{N}\sum_{j=1}^{C}(u_{ij})^m \mathrm{d}(\vec{\boldsymbol{x_i}}, \vec{\boldsymbol{v_j}}) + \sum_{i=1}^{N}(u_{i,C+1})^m\delta\right] + \lambda\left[\sum_{i=1}^{N}\sum_{j=1}^{C}\sum_{j\in N_j}\beta(u_{ij}-u_{ij'})^2\right] \tag{11}$$

.

The term E in (11) refers to the energy of the pixel for the membership value u_{ij}. The rest of the terms in (11) are already defined in section 2. The optimization of (11) is done using the simulated annealing (Mather, P. and Tso, B., 2010). Objective functions of the $\mathrm{FNC}_{\mathrm{D}i}$ classifiers for $i = 1, \ldots, 4$ are formed by replacing the APF, i.e. the term $\beta(u_{ij} - u_{ij'})^2$ in equation (11) with the corresponding APFs being equal to $-\gamma \exp \frac{-\eta^2}{\gamma}$, $\frac{-\gamma}{\left[\frac{1}{1+\frac{\eta^2}{\gamma}}\right]^2}$, $\gamma \ln\left(1+\frac{\eta^2}{\gamma}\right)$ and $\gamma|\eta| - \gamma^2 \ln\left(1+\frac{|\eta|}{\gamma}\right)$, respectively (Li, 2009). In this way, $\mathrm{FNC_S}$ and the $\mathrm{FNC}_{\mathrm{D}i}$ represent the hybrid classifiers obtained by using the S and DA_i MRF models for $i = 1, \ldots, 4$, respectively.

The term λ is used in the objective function of the hybrid classifier to balance the contribution of information from the spectral and spatial domains. This further controls the impact of spatial and spectral information on the classification. The weights β control the amount of influence that a site has with its neighbours.

3.2. *Fuzzy noise classifier parameter estimation*

The outputs of FNC are fractional images, where each pixel depicts the membership values i.e. the possibilistic percentage cover of a particular class within that pixel. The classifier generates a fractional image for each individual class.

Estimation of the FNC parameter, which includes the noise distance (δ) and the fuzzification factor (m), is essential for ensuring the best performance of the FNC. The parameter combination which gives the maximum classification accuracy for the FNC were considered. Accuracy of the fuzzy classification was assessed by minimizing the entropy associated with the fractional images (Dehghan and Ghassemian, 2006). Entropy minimization is a widely accepted method to quantify the uncertainty associated with an image. To calculate the entropy of a class, random pixels were selected from the high membership regions of the fractional image for each class. Vectors of membership values were formed for each pixel by combining membership values from all the fractional images. For each such membership vector, the entropy was calculated using equation (12) and was averaged to obtain the entropy for a pixel.

$$\mathrm{H_{avg}} = \frac{\sum_{i=1}^{C} (u_{ij}) \log_2 (u_{ij})}{\sum_{i=1}^{C} (u_{ij})} \tag{12}$$

Entropy as the sole criterion for optimal parameter estimation, was found to be insufficient, as the minimum entropy fractional images could possibly be generated from a parameter combination, that resulted in an inaccurate classification. To address this problem, accuracy estimation was done using inter-class membership change calculation (IMC) which exploits the fact that, in the optimal classification, membership value of the class pixels will be highest in the fractional image associated with that class only, but corresponding pixel membership values will be lowest in the other fractional images (Townsend and Philip, 2000). In this method, emphasis is given on finding parameters that maximize this difference in membership values for all class pixels. To do so, the difference is calculated for a fractional image between the mean membership values at known class locations, and the mean of membership values at known non-class locations. A large difference corresponds with a high is the classification accuracy. The FNC estimates were found by minimizing the entropy of the fractional image at the same time, maximizing the IMC.

3.3. *Hybrid classifier parameter estimation*

The hybrid classifier was developed, by adding a spatial term to the FNC formulation. For the hybrid classifier, two parameters need to be estimated. The first is the weight factor with $0 \leq \lambda \leq 1$, which controls the impact of spatial and spectral component. The second is β in case of S-MRF or γ in case of a DA-MRF. Both parameters have an impact on the classification accuracy, and hence their estimation is critical.

The main objective behind the used of DA models was to preserve the class boundaries during classification. Hence the preservation of class boundaries, was considered as the main criteria for hybrid parameter estimation. To find the optimal parameter values, the classification was repeated with different combination of λ and β in case of S-MRF and λ and γ in case of DA-MRF. The range of β was set to [1, 10] and that of γ to [0,1], as values outside this range were found to reduce the overall classification accuracy drastically.

Edge preservation in the fractional images was quantified in this study using the mean-variance method (Chawla, 2010; Singha et al., 2015). This method considers the mean difference in membership values across boundaries as well as the membership variance on either side of boundaries as a means to quantify the edge preservation in the fractional images. Fractional images with the highest mean difference in membership values across boundaries and minimum membership value variance on either side of the boundaries provided the best results in terms of edge preservation. Ultimately the parameter combination which provided the highest edge preservation in the classification result, was considered as the hybrid classifier parameter estimates.

Once the FNC and hybrid classifier parameters were estimated, the optimal membership values, and hence the fractional images, were found by minimizing equation (11) using simulated annealing (SA) optimization (Mather, P. and Tso, B., 2010; Geman and Geman, 1984). When using SA, the initial temperature (T_0) was set to 3 and the temperature update rate (k) was set to 0.90 for efficient optimization. These values were considered because the variance in the estimates were minimal on repeating the estimation (Tolpekin and Stein, 2009).

3.4. *Accuracy assessment*

To quantify the accuracy of fuzzy classifiers the error matrix that is commonly applied for hard classification cannot be used. In this study we used the Fuzzy error matrix (FERM) (Zhang and Foody, 1998). It is similar to the error matrix, but it takes fractional images as its input. Hence the cell values are between 0 and 1. This is based on MIN operator (Intersection operator) which shows the maximum possible overlap between reference and classified image and is calculated as shown in equation (13) (Silván-Cárdenas and Wang, 2008). In equation (13), u_{ij} and v_{ij} represent membership value of the i^{th} pixel in fractional image for class j, in the assessed image and reference image, respectively.

$$\mathrm{P}_{\mathrm{n}_{ij}} = \mathrm{MIN}(u_{ij}, v_{ij}) \tag{13}$$

The efficiency of the novel hybrid classifier was obtained by evaluating its performance on coarse resolution (56 m) AWiFS and medium resolution (23.5 m) LISS-III images. Fractional images generated from high resolution (5.6 m) LISS-IV image values were used as the reference image. For the accuracy assessment, the cell resolutions of AWiFS, LISS-III and LISS-IV images were resampled to make their resolutions in the ratio 1:4:12. Hence 16 pixels (4 × 4) of LISS-III and 144 pixels (12 × 12) of AWiFS were combined (pixel values averaged) to reach the pixel dimension of LISS-IV image. In this way, an effective comparison could be made between the images with different resolutions. Resampling of the images and aggregation of pixels values were potential sources of error, but were ignored in this study since they were likely to be very small. We applied nearest neighbour resampling resulting in geometric discontinuities in the order of plus or minus half the pixel size, which is considered to be acceptable (Schowengerdt, 2006).

4. Study Area & Data

The study area is the Sitarganj Tehsil, Udham Singh Nagar District, Uttarakhand State, India, located at 280 52′ 29″ N to 280 54′ 20″ N and 790 34′ 25″ E to 790 36′ 34″ E. Uttarakhand is a state in the northern part of India and Sitarganj Tehsil is located in the southern part of the state. Sitarganj Tehsil is near Pand Nagar Agricultural University, famous for its participation in the Green Revolution of India. The study area was selected for its diversity in classes. The current research aims at testing the capability of a novel classifier; and Sitarganjs Tehsil has a large diversity of distinguishable classes. Six classes were identified from the study area and are labeled in Figure 3. The study area mostly has sugarcane and paddy agricultural farms. It also has two big reservoirs named Dhora and Bhagul on the north western and south eastern parts respectively. Images from AWiFS and LISS-III sensors onboard Resourcesat-1 were used for studying the efficiency of the novel hybrid classifier considered in this work. The AWiFS (56 m), LISS-III (23.5 m) and LISS-IV (5.8 m) images were acquired on the same date i.e., 15 October 2007, and hence are well comparable. The validation of classification was done against the LISS-IV image of the same area. In this study, the LISS-IV image was rectified using Survey of India (SOI) toposheet numbered, $53P/9$. The geo-registration of the AWiFS and LISS-III images were conducted using the geometrically corrected LISS-IV image. Figure 3 shows the high resolution, LISS-IV, image of the study area. The AWiFS images and LISS-III image provides the low resolution and medium resolution images of the same area.

Ground data validation was not preferred in this study, as it is difficult to identify a pixel area on the ground. Also it is not effective idea to manually quantify the percentage cover of a particular class within the area on ground, as the certainty to which the classes could be identified is a subjective issue (Foody, 2000).

5. Results

5.1. *Fuzzy noise classifier parameter estimates*

Parameters for both the FNC and the hybrid classifier were estimated separately for each image considered in this study. On analyzing the FNC results for different parameter values, the δ was found to have minimal or no impact on the value of total entropy or IMC beyond the threshold $\delta = 10000$. For $\delta < 100$, unrealistic classification emerged, and so these values were avoided. Figure 4 shows the effect of $\delta > 100$ on m for the 'Agricultural Field With Crop' class in AWiFS image. As can be observed, estimated m values are least affected by changes in δ beyond $\delta = 10000$. So m was estimated, keeping $\delta = 10000$. Estimation was done separately for each fractional image (or class) generated by FNC.

The FNC parameters were estimated with the help of the normalized entropy graph and the IMC graph, as shown in figure 5. In particular, the entropy versus

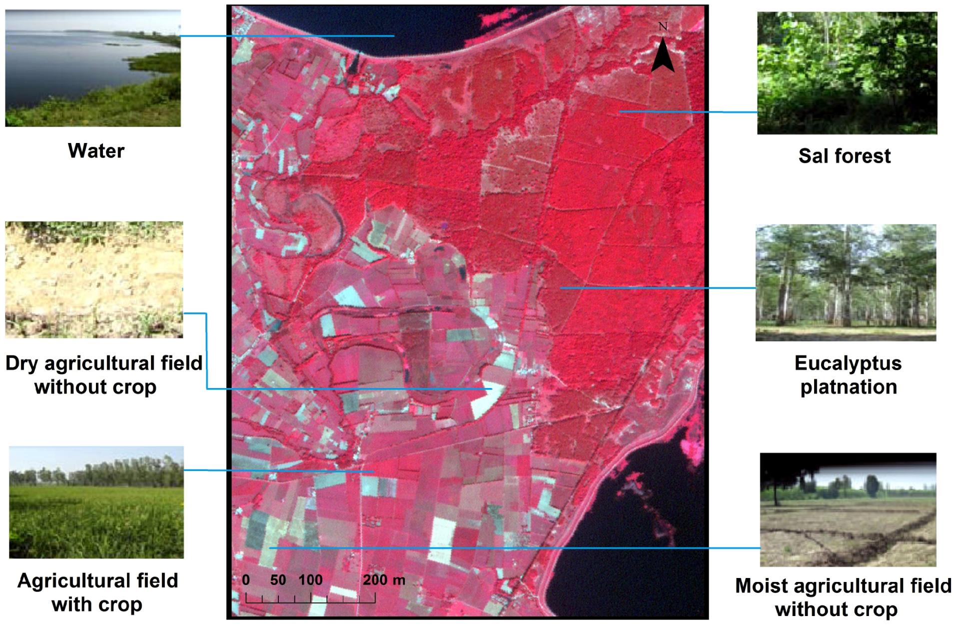

Figure 3.: LISS-4 imagery (from Resourcesat-1) of Sitarganjs Tehsil, Udham Singh Nagar District, Uttarakhand State, India, aquired on 15 October 2007. The image is the FCC image with 0.77 - 0.86 µm spectral band mapped to the Red band, The image is the FCC image with 0.62 - 0.68 µm spectral band mapped to the Green, and the 0.52 - 0.59 µm spectral band mapped to Blue band.

IMC graph of the AWiFS image is shown in Figure 5. Mean m estimates, obtained for AWiFS and LISS-III images, are shown in Table 1. Optimal m values estimation for the reference image i.e. LISS-IV, was also essential to obtain the best possible soft reference data. For LISS-IV image, the optimal m value was found to be 3.0. Visual inspection of the optimal fractional images generated using the estimated parameter values showed them to be very accurate, and this added to the confidence in the estimates.

Table 1.: Fuzzification factor m estimates obtained against the low, medium and high spatial resolution (reference) images for the FNC

Image	**Fuzzification factor** (m)
AWIFS	2.7
LISS-III	2.9

From Table 1, one may notice that m shows a slight increasing trend with increase in the spatial resolution of the images, which in turn is caused by the increase in entropy of an image with an increase in its resolution. This is just an observation which has been made and has no impact on the results of this study.

5.2. *Hybrid classifier parameter estimates*

Parameter estimates for the hybrid classifier were obtained against the fractional images set quantified to have the maximum edge preservation. Quantification of

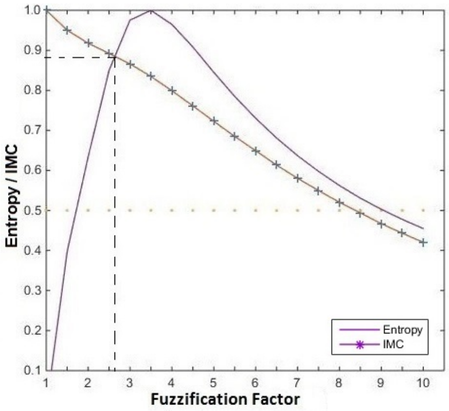

(a) $\delta = 100$

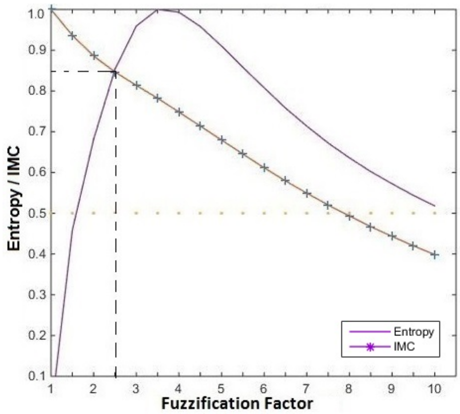

(b) $\delta = 1000$

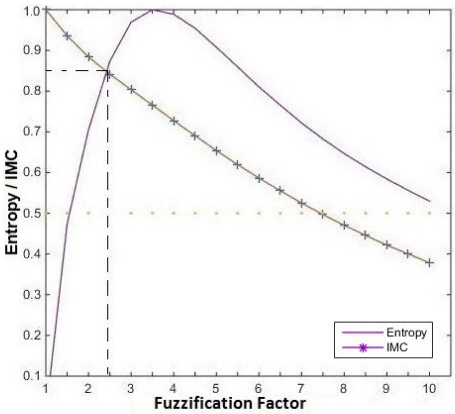

(c) $\delta = 10000$

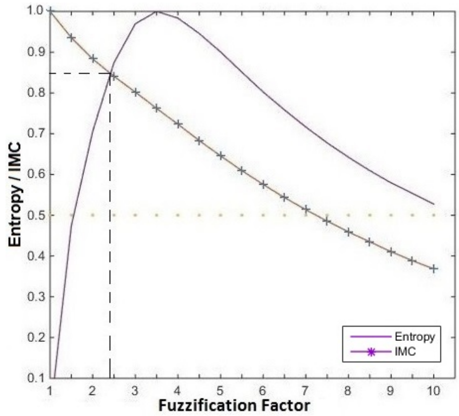

(d) $\delta = 50000$

Figure 4.: Effect of δ on estimation of m for the Agricultural Field With Crop class in AWiFS image, for different values of δ

edge preservation in the fractional images was conducted using mean-variance method as explained in the sub-section 3.3. Estimates for the hybrid classifier obtained for the low spatial resolution - AWiFS, and medium spatial resolution - LISS-III images, for different MRF models are shown in Table 2.

Table 2.: The hybrid classifier estimates obtained against the low and medium spatial resolution images

Hybrid Classifier	MRF Model	AWiFS		LISS-III	
		λ	β/γ	λ	β/γ
$\mathrm{FNC_S}$	S	0.6	5.0	0.9	5.0
$\mathrm{FNC_{D1}}$	$\mathrm{DA_1}$	0.9	0.4	0.9	0.5
$\mathrm{FNC_{D2}}$	$\mathrm{DA_2}$	0.7	0.8	0.8	0.4
$\mathrm{FNC_{D3}}$	$\mathrm{DA_3}$	0.7	0.9	0.8	0.5
$\mathrm{FNC_{D4}}$	$\mathrm{DA_4}$	0.8	0.8	0.9	0.7

As was the case with FNC parameter estimation, the hybrid parameters were estimated for the high spatial resolution reference image i.e. LISS-IV also, to generate the optimal soft reference data. The hybrid parameter estimates for LISS-IV image is shown in Table 3.

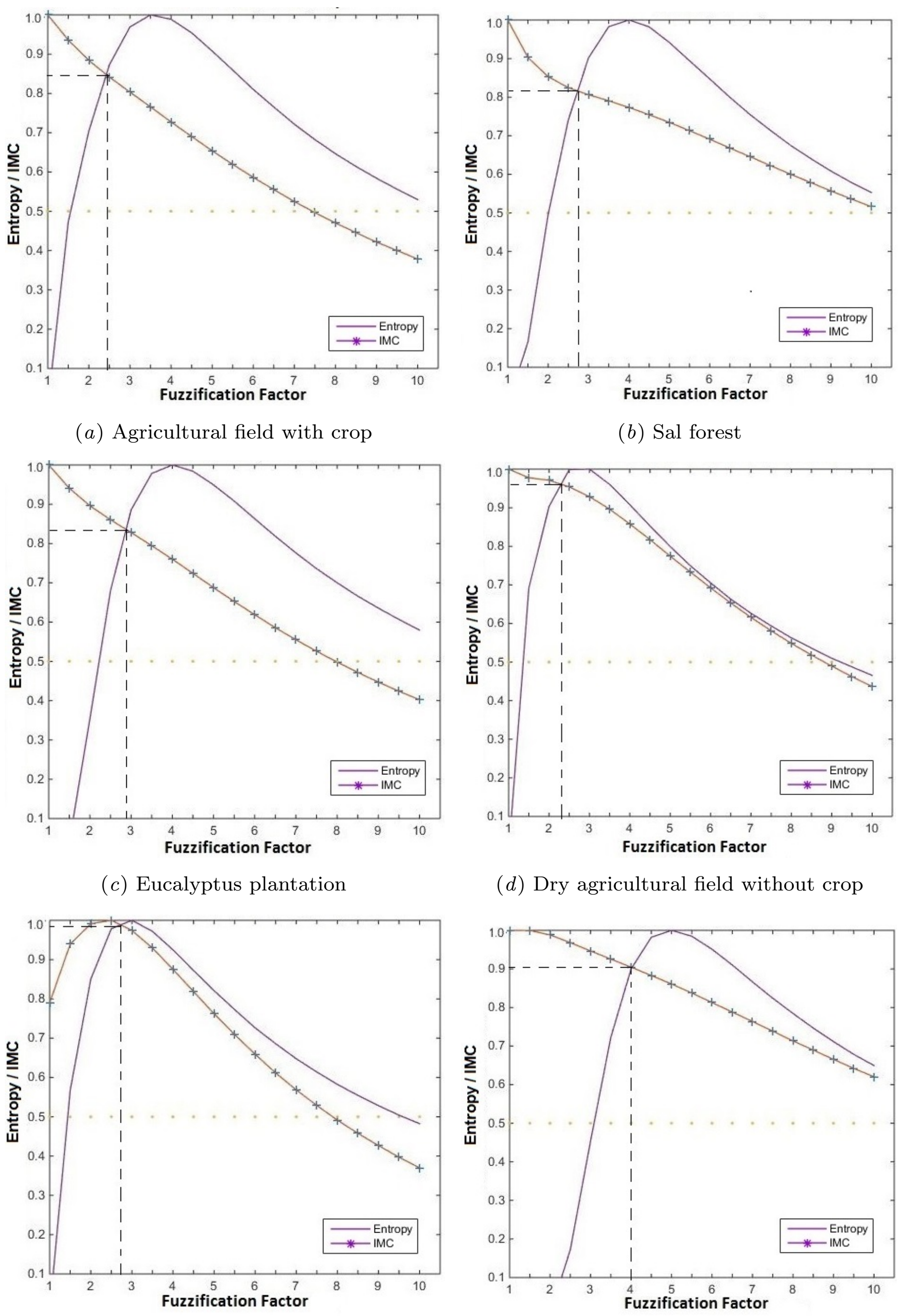

(*a*) Agricultural field with crop (*b*) Sal forest

(*c*) Eucalyptus plantation (*d*) Dry agricultural field without crop

(*e*) Moist agricultural field without crop (*f*) Water

Figure 5.: Entropy/IMC Vs Fuzzification Factor plots for different LULC classes considered in the AWiFS image

Among the different DA-MRF prior models used in this study, combination of the DA_4 model with the FNC, i.e. the FNC_{D4} classifier, showed the maximum edge preservation capability. This was observed for all the three images considered in this study. Figures 6 and 8 show the fractional images generated by FNC for AWiFS and LISS-III images respectively, whereas fractional images generated by the FNC_{D4} classifier for AWiFS and LISS-III images are shown in figure 7 and figure

Table 3.: The hybrid classifier estimates obtained against the high spatial resolution reference images

Hybrid Classifier	MRF Model	LISS-IV λ	LISS-IV β/γ
FNC_S	S	0.6	6.0
FNC_{D1}	DA_1	0.9	0.4
FNC_{D2}	DA_2	0.7	0.5
FNC_{D3}	DA_3	0.7	0.7
FNC_{D4}	DA_4	0.8	0.5

9 respectively. In the case of FNC_{D4} classifier, the membership values of unrealistic isolated pixels have been reduced, thus achieving a more realistic classification. The FNC_{D4} classifier achieves this by selective smoothening of pixels as explained in section 3. Also a reduction in the accuracy is observed for fractional images produced for the AWiFS image when compared to that of LISS-III image, caused by the lower resolution of AWiFS as compared to LISS-III.

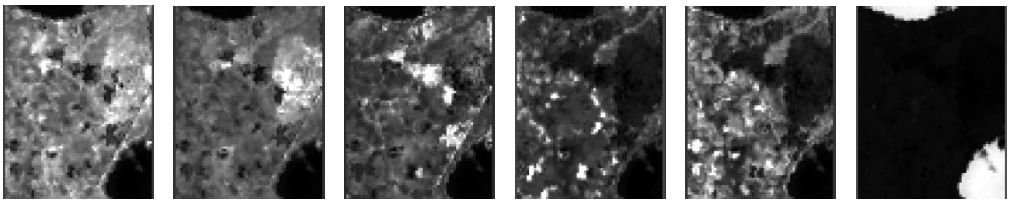

(a) (b) (c) (d) (e) (f)

Figure 6.: Fractional Images obtained against AWiFS image for the FNC, (a) for Agriculture fields with crop, (b) Sal Forest, (c) Eucalyptus plantation, (d) Dry agricultural field without crop, (e) Moist agricultural field without crop, and (f) Water.

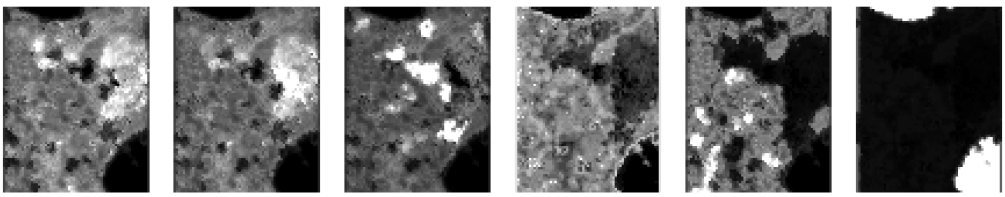

(a) (b) (c) (d) (e) (f)

Figure 7.: Fractional Images obtained against AWiFS image for the FNC_{D4} classifier, (a) for Agriculture fields with crop, (b) Sal Forest, (c) Eucalyptus plantation, (d) Dry agricultural field without crop, (e) Moist agricultural field without crop, and (f) Water.

5.3. *Accuracy assessment results*

Table 4 shows the FERM overall fuzzy accuracy of classification results for AWiFS against LISS-IV reference images and LISS-III against LISS-IV reference images for FNC, FNC_S, FNC_{D1}, FNC_{D2}, FNC_{D3} and FNC_{D4} classifiers.

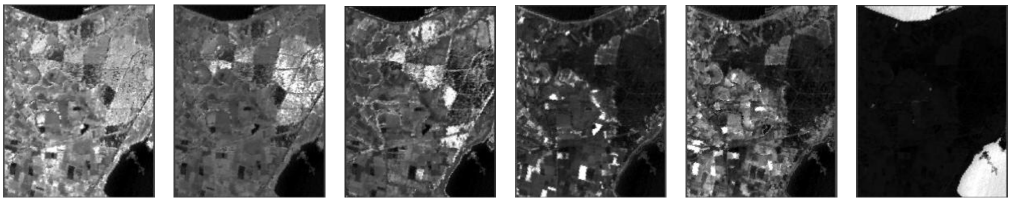

(a) (b) (c) (d) (e) (f)

Figure 8.: Fractional Images obtained against LISS-III image for the FNC, (a) for Agriculture fields with crop, (b) Sal Forest, (c) Eucalyptus plantation, (d) Dry agricultural field without crop, (e) Moist agricultural field without crop, and (f) Water.

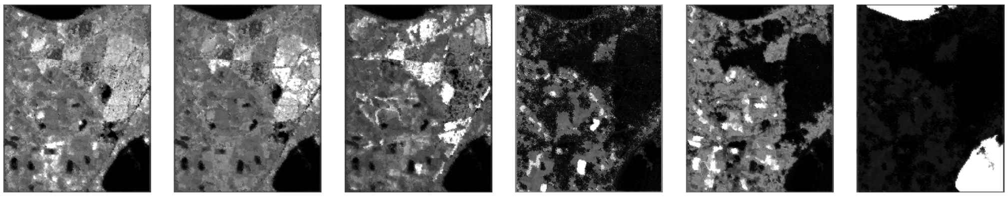

(a) (b) (c) (d) (e) (f)

Figure 9.: Fractional Images obtained against LISS-III image for the $\mathrm{FNC_{D4}}$ classifier, (a) for Agriculture fields with crop, (b) Sal Forest, (c) Eucalyptus plantation, (d) Dry agricultural field without crop, (e) Moist agricultural field without crop, and (f) Water.

Table 4.: FERM Overall fuzzy accuracy obtained on comparing the low and medium spatial resolution fractional images with the high resolution reference fractional image, for the trained case

Classifier	Accuracy (%)	
	AWiFS Vs LISS-IV	LISS-III Vs LISS-IV
FNC	83.2	87.3
$\mathrm{FNC_S}$	82.7	88.2
$\mathrm{FNC_{D1}}$	84.6	87.6
$\mathrm{FNC_{D2}}$	81.8	77.0
$\mathrm{FNC_{D3}}$	81.4	75.6
$\mathrm{FNC_{D4}}$	87.3	89.4

Among the different classifiers formed, $\mathrm{FNC_{D4}}$ gave the highest overall fuzzy accuracy of 87.3% for AWiFS and 89.4% LISS-III images respectively. The APF functions are usually convex, and there exist a region of η within which the smoothing strength therefore increases monotonically with increase in $|\eta|$. A perfectly convex APF function will cause no smoothening at the boundaries, and the smoothening strength gradually increases on moving away from the boundaries. This way of smoothening blends well with the concept of gradual class variation at the boundaries in natural objects. The APF of $\mathrm{DA_4}$ is a more smooth convex function than the APF's of its counterparts (Li, 2009) and therefore performs better. It can be observed that the use of S, $\mathrm{DA_2}$ and $\mathrm{DA_3}$ MRF models for spatial contextual modelling resulted in a slight reduction in the accuracy of the FNC for the all the images considered in this study. Also, while acquiring higher spatial resolution data by a sensor, intra pixel neighbour-reflectance effect is caused due to a single class, whereas in coarser spatial images the intra pixel neighbour-reflectance effect is caused due to an increased number of classes. This neighbour effect is added as noise to a pixel. Hence the coarser pixels have a stronger neibhour pixel effect than the high resolution pixels. For the same reason, the DA_4 produces more improvement in accuracy for the AWiFS image than for the LISS-III image.

5.4. *Performance with untrained classes*

The FNC considers any class other than the classes of interest as image noise. To quantify the robustness of FNC to noise, a class was deliberately avoided while training the classifier and the performance of the classifier was then evaluated i.e., the classifier was deprived of the signature information about one known class and classification was done. The results obtained for one such experiment are shown in Table 5.

Table 5.: Fuzzy users accuracy obtained for the trained and untrained cases, for low and medium spatial resolution images

Classifier	Accuracy (%)			
	AWiFS Vs LISS-IV		LISS-III Vs LISS-IV	
	Untrained	Trained	Untrained	Trained
FNC	74.8	84.0	77.2	88.2
FNC_S	75.6	85.7	76.3	88.5
FNC_{D4}	55.0	64.9	69.4	75.4

Here the class 'Agricultural field with Crop' was left untrained for both AWiFS and LISS-III images. Table 5 compares the user accuracy of FNC, FNC_S and FNC_{D4} classification results for AWiFS and LISS-III images for both the trained and the untrained case, using the FNC_{D4} classifier. The other hybrid classifiers were not considered for this analysis, as they were having relatively low accuracy when compared with the FNC_{D4} classifier. It can be seen from Table 5 that the user accuracy obtained in the presence of an untrained class was lower, when compared to the user accuracy if all classes were trained. For the AWiFS data, the decrease in user accuracy in the untrained case were equal to 9.2%, 10.1% and 9.9% for FNC, FNC_S and FNC_{D4}, respectively. For the LISS-III data, the decrease in user accuracy for untrained case were 11.0%, 12.2% and 6.0% for FNC, FNC_S and FNC_{D4} respectively. The decrease in user accuracy for untrained case is caused due to the increased number of untrained classes, which gets added to the pixel as noise. Even though the FNC clearly has the ability to restrict the information flow from untrained classes in an image, the results from Table 5 shows that the performance of FNC classifiers decreases when there is an increase in noise. The relatively small drop in user accuracy for AWiFS as compared to LISS-III can be explained by the intra-pixel neighbourhood reflectance effect, as explained in section 5.3.

5.5. *Comparison with results of previous studies*

In various studies, the information from the spectral, spatial and temporal domains has been used, in all possible permutations, to achieve better image classification.

Among these, the studies conducted for evaluating the impact of incorporating spatial contextual information, modelled using MRF in combination with fuzzy c-Means classification (FCM) (Singha et al., 2015), and that with possibilistic c-means classification (Chawla, 2010) are studies which are closely related to that of ours. Also, they both have used the same datasets that were used for this study.

The results of these studies were compared with those of the FNC-MRF classifier. In case of FCM, the $\mathrm{DA}_3 - \mathrm{MRF}$ prior gave the best result and the overall fuzzy accuracy for AWiFS and LISS-III images were 85.5% and 89.5% respectively (Singha et al., 2015). In the case of PCM, $\mathrm{DA}_2 - \mathrm{MRF}$ prior proved to be the best and its overall fuzzy accuracy for AWiFS and LISS-III images were 82.0% and 87.3% respectively (Chawla, 2010). Upon comparing the overall fuzzy accuracy of $\mathrm{FNC_{D4}}$ with $\mathrm{FCM_{D3}}$, one can see that there is an improvement in accuracy of 1.8% for AWiFS image for $\mathrm{FNC_{D4}}$ but almost the same for LISS-III image. When comparing the overall fuzzy accuracy of $\mathrm{FNC_{D4}}$ with $\mathrm{PCM_{D2}}$, one can see that there is an improvement in accuracy of 5.3% and 2.1% for $\mathrm{FNC_{D4}}$ against AWiFS and LISS-III images respectively. This proves the ability of the FNC to produce better classification results, when supported with spatial contextual information.

6. Discussion

The hybrid classifiers developed in this study combines the DN value of a pixel from the spectral domain with the context of the pixel in the spatial domain. The spatial contextual information for a pixel was modelled using four different discontinuity adaptive MRF models, and the impact of adding information onto the FNC was studied. Mathematically, the FNC is expressed as an optimization function, and hybrid classifiers were created by adding the APF's of the MRF models as additional terms in the objective function. The weight factor, λ allowed to control the contribution from the spatial and spectral terms of the hybrid classifier. For $\lambda = 0$, the spatial context of a pixel does not affect the classification, whereas for $\lambda = 1$, classification will be performed based on the spatial context of a pixel. The optimal value of λ was found to be dependent on the resolution of the image and was estimated using methods in section 3.3.

The MRF helps in achieving better classification by smoothening the unrealistic pixel locations in an image, thus addressing the isolated pixel problem. The DA-MRF model ensures that the smoothening happens only within a class and not at the class boundaries. As a result, the final fractional images produced by the hybrid classifier looks more like a smoothened version of the original FNC outputs, resulting in a small decrease in the classification accuracy. But the increase in accuracy obtained by reducing the isolated pixel problem and the mixed pixel problem outnumbers this decrease due to increased smoothness. Each MRF has a unique AIF, and as a result their effectiveness in spatial contextual modelling, was different even for the same image. Since there exists no method to predict the prospectiveness of using an MRF model for an image, spatial modelling was done using all five MRF models to compare their performance and thus identify the best model. The parameters associated with these models such as β and γ were also found to be data dependent and to have an impact on the classification accuracy. The hybrid classifier parameter estimates were the values that produced the highest edge preservation in the classification result.

FNC has clearly the ability to restrict the information flow from untrained classes (non-interested classes) in an image. For each hybrid classifier considered in this study, the presence of untrained classes in the input image caused a decrease in the classification accuracy.This is because the untrained classes gets added to the pixel as noise. Whatsoever, there is an 14.1% improvement in the classification accuracy of FNC_{D4} as compared to the classification done by the FCM_{D3} classifier, for the LISS-III image (Singha et al., 2015). This clearly shows robustness of the FNC_{D4} classifier, to the presence of untrained classes in the image as compared to the PCM or FCM based hybrid classifier. Hence the FNC_{D4} classifier should be preferred in case there are untrained classes or unrealistic isolated pixels in the input image.

The current study was conducted on low resolution (AWiFS) and medium resolution (LISS-III) images only. Within the scope of the images used in this study, it was found that the FNC_{D4} classifier, which uses the DA_4 MRF model, is the best. This is because the APF of DA_4 is a more smooth convex function with no smoothening at the boundaries and the smoothening strength gradual decreases on moving away from the boundaries. The kind of smoothening blends well with the concept of gradual class variation at the boundaries in the nature. The fuzzy nature of the FNC enabled the hybrid classifier to address the mixed pixel problem, whereas the use of spatial contextual information helped in addressing the isolated pixel problem, thus making the FNC_{D4} more efficient than the FNC. But still to confirm the general usability of this classifier in remote sensing studies, its classification accuracy has to be evaluated for other resolution images with different set of classes as well, but investigating on this is left to future studies.

7. Conclusion

The paper studied the effect of adding spatial contextual information to a spectral classifier. A supervised version of noise clustering was used in this study, as the spectral classifier. Modelling of the spatial contextual information at the pixel level was achieved using MRF technique. Both coarse (AWiFS) and medium resolution (LISS-III) images from Resourcesat-1 were used for evaluating the performance of the novel hybrid FNC_{DA} classifier. Among the different discontinuity adaptive MRF models used, the FNC_{D4} classifier was found to provide the highest classification accuracy for both the images. The overall FERM accuracy for FNC_{D4} classifier were found to be 87.3% and 89.4% respectively, for the AWiFS and LISS-III images. Classification was also conducted by keeping a class untrained, to study the effects of undesirable classes which are present in an image, on the FNC_{DA} accuracy. In that case, a decreases in user accuracy of 9.9% and 6.0% were observed for AWiFS and LISS-III respectively, as compared to the fully trained case. The study concludes that the use of spatial contextual information improved the classification accuracy of the fuzzy noise classifier (FNC), when compared to the accuracy obtained on using FCM or PCM in its place.

References

Bezdek, J. C., Ehrlich, R., and Full, W., 1984, FCM: The fuzzy c-means clustering algorithm., Computers and Geosciences, 10.2, 191-203.

Binaghi, E., Brivio, P. A., Ghezzi, P. and Rampini, A., 1999, A fuzzy set-based accuracy assessment of soft classification., Pattern recognition letters, 20.9, 935-948.

Chawla, S., 2010, Possibilistic c-Means-Spatial Contextual Information based sub-pixel classification approach for multi-spectral data. University of Twente, Faculty of Geo-Information and Earth Observation (ITC), Enschede.

Congalton, R. G., 1991, A review of assessing the accuracy of classifications of remotely sensed data., Remote sensing of Environment, 37.1, 35-46.

Dave', R. N., 1991, Characterization and detection of noise in clustering., Pattern Recognition Letters, 12, 657-664.

Dave', R. N., 1993, Robust fuzzy clustering algorithms, Second IEEE International Conference on Fuzzy Systems., San Francisco, CA, 28 Mar 1993 - 01 Apr 1993, 2, 1281-1286.

Dave', R. N. and Krishnapuram, R., 1997. Robust clustering methods: a unified view., IEEE Transactions on Fuzzy Systems, 5.2, 270-293.

Derin, H., and Elliott, H., 1987 Modeling and segmentation of noisy and textured images using Gibbs random fields., IEEE Transactions on Pattern Analysis and Machine Intelligence, 9.1: 39-55.

Dehghan, H. and Ghassemian, H., 2006, Measurement of uncertainty by the entropy: application to the classification of MSS data., International journal of remote sensing, 27.18, 4005-4014.

Dubes, R.C., and Jain A.K., 1989, Random field models in image analysis., Journal of applied statistics 16.2 : 131-164.

Foody, G. M., 1997, Fully fuzzy supervised classification of land cover from remotely sensed imagery with an artificial neural network., Neural Computing and Applications, 5.4, 238-247.

Foody, G. M., 2000, Estimation of sub-pixel land cover composition in the presence of untrained classes., Computers and Geosciences, 26.4, 469-478.

Geman, S., and Geman, D., 1984, Stochastic relaxation, Gibbs distributions, and the Bayesian restoration of images., IEEE Transactions on Pattern Analysis and Machine Intelligence 6.6, 721-741.

Green, K. and Congalton, R. G., 2004, An error matrix approach to fuzzy accuracy assessment: The NIMA Geocover Project, Boca Raton, FL: CRC Press., eBook ISBN: 978-0-203-49758-6.

Krishnapuram, R. and Keller, J. M., 1993, A possibilistic approach to clustering., IEEE Transactions on Fuzzy Systems, 1.2, 98-110.

Krishnapuram, R. and Keller, J. M., 1996, The possibilistic c-means algorithm: insights and recommendations., IEEE Transactions on Fuzzy Systems, 4.3, 385-393.

Li, S. Z., 1995, On discontinuity-adaptive smoothness priors in computer vision., IEEE Transactions on Pattern Analysis and Machine Intelligence, 17, 576-586.

Li, S. Z., 2009, Markov random field modeling in image analysis, Springer., ISBN: 978-1-84800-279-1.

Mather, P. and Tso, B., 2010, Classification methods for remotely sensed data, CRC press., ISBN: 9781420090727.

Magnussen, S., Boudewyn, P., and Wulder, M., 2004, Contextual classification of Landsat TM images to forest inventory cover types., International Journal of Remote Sensing, 25.12 : 2421-2440.

Pontius Jr., R. G., and Cheuk, M. L., 2006, A generalized crosstabulation matrix to compare softclassified maps at multiple resolutions., International Journal of Geographical Information Science, 20.1, 1-30.

Silván-Cárdenas, J., and Wang, L., 2008, Sub-pixel confusionuncertainty matrix for assessing soft classifications. Remote Sensing of Environment, 112.3, 1081-1095.

Singha, M., Kumar, A., Stein, A.,Raju, P. N. L., and Murthy, Y. K., 2015, Importance of DA-MRF Models in Fuzzy Based Classifier, Journal of the Indian Society of Remote Sensing: 1-9.

Tolpekin, V. A., and Stein, A., 2009, Quantification of the effects of land-cover-class spectral separability on the accuracy of Markov-random-field-based superresolution mapping., IEEE Transactions on Geoscience and Remote Sensing, 47.9, 3283-3297.

Townsend, P. A., 2000, A quantitative fuzzy approach to assess mapped vegetation classifications for ecological applications., Remote Sensing of environment, 72.3: 253-267.

Tso, B and Olsen, R.C., 2005, Combining spectral and spatial information into hidden Markov models for unsupervised image classification, International Journal of Remote Sensing, 26.10: 2113-2133.

Zadeh, L. A., 1965, Fuzzy sets, Information and control, 8.3, 338-353.
Zhang, J. and Foody, G., 1998, A fuzzy classification of sub-urban land cover from remotely sensed imagery. International Journal of Remote Sensing, 19.14, 2721-2738.